arXiv:1612.01509v1 [quant-ph] 5 Dec 2016

Regularity and chaos in cavity QED

Miguel Angel Bastarrachea-Magnani[1,2]‡, Baldemar López-del-Carpio[3], Jorge Chávez-Carlos[2], Sergio Lerma-Hernández[2,3]§ and Jorge G. Hirsch[2]‖.

[1] Physikalisches Institut, Albert-Ludwigs-Universitat Freiburg, Hermann-Herder-Str. 3, Freiburg, Germany, D-79104.
[2] Instituto de Ciencias Nucleares, Universidad Nacional Autónoma de México, Apdo. Postal 70-543, Cd. Mx., México, C.P. 04510
[3] Facultad de Física, Universidad Veracruzana, Circuito Aguirre Beltrán s/n, Xalapa, Veracruz, México, C.P. 91000

E-mail: miguel.bastarrachea@nucleares.unam.mx, ramedlab1@gmail.com, fis_jorge.chavez@yahoo.com.mx, slerma@uv.mx, and hirsch@nucleares.unam.mx

Abstract. The interaction of a quantized electromagnetic field in a cavity with a set of two-level atoms inside can be described with algebraic Hamiltonians of increasing complexity, from the Rabi to the Dicke models. Their algebraic character allows, through the use of coherente states, a semiclassical description in phase space, where the non-integrable Dicke model has regions associated with regular and chaotic motion. The appearance of classical chaos can be quantified calculating the largest Lyapunov exponent in the whole available phase space for a given energy. In the quantum regime, employing efficient diagonalization techniques, we are able to perform a detailed quantitative study of the regular and chaotic regions, where the quantum Participation Ratio (PR) of coherent states on the eigenenergy basis plays a role equivalent to the Lyapunov exponent. It is noted that, in the thermodynamic limit, dividing the Participation Ratio by the number of atoms leads to a positive value in chaotic regions, while it tends to zero in the regular ones.

PACS numbers: 03.65.Fd, 42.50.Ct, 64.70.Tg

Keywords: chaos, Dicke model, Lyapunov exponent, Participation Ratio, Husimi function.

Submitted to: *Phys. Scr.*

‡ On postdoctoral leave from Instituto de Ciencias Nucleares, Universidad Nacional Autónoma de México
§ On sabbatical leave from Facultad de Física, Universidad Veracruzana.
‖ Correspondence author.

1. Introduction

The problem of how isolated quantum many-body systems could attain a state of equilibrium and its dynamical implications in the field of quantum thermodynamics, has become a fundamental issue where many challenging questions remain open [1, 2, 3, 4]. It has been shown that in a quantum systems equilibration can occur for unitary dynamics under conditions of classical chaos [5]. So, quantum chaos [6, 7, 8], the study of quantum systems which have a classical chaotic counterpart [9, 10, 11, 12], has become a very important topic in this context. Typically, classical many-body systems containing a big number of degrees of freedom tend to have chaos as they are non-integrable, i.e. they do not have as much conserved quantities as degrees of freedom. In the classical realm, non-integrability, chaos and ergodicity are intimately related. However, these definitions fail to capture the quantum realm due to the lack of trajectories in the quantum phase space.

Algebraic Hamiltonians provide a natural scenario to explore these subjects. The algebra gives a simple way to build coherent states. Being considered the most classical quantum states, they provide a simple connection between the quantum and classical realms. The Dicke model [13] is an algebraic Hamiltonian which has gained interest in the last years thanks to its combination of algebraic simplicity and interesting phenomena. It was meant to describe a collective system of $\mathcal{N}$ atoms within the two-level approximation interacting with a single mode of radiation field inside a QED cavity. However, its algebraic simplicity makes it suitable to describe interacting qubits systems within the quantum information framework. From Bose-Einstein condensates in optical lattices, to polaritons, and superconducting qubits in circuit QED, the Dicke model has become a paradigmatic example of quantum collective behavior [14, 15, 16, 17, 18, 19, 20, 21, 22].

As a toy model, the Dicke Hamltonian is a good start for several approximated Hamiltonians and to different approaches to describe quantum systems. Particularly, the model is well-known thanks to its superradiant thermal phase transition that persists in the zero-temperature, giving rise to a quantum phase transition (QPT) [23, 24, 25, 26, 27]. In connection to the ground-state QPT it has other interesting features like entanglement [28, 29], and the excited-state quantum phase transitions (ESQPT) [30, 31, 32, 33]. Also, very important for this work, it presents quantum chaos. The Dicke model describes one of the simplest nonintegrable atom-field system, exhibiting quantum chaos. In the Dicke model the evolution equation of the Husimi function is of the Fokker-Planck type, and the transition from ergodic to non-ergodic behavior can be quantified employing the average over an energy shell of the inverse participation ratio between the eigenstates of the integrable and the total Hamiltonian. In this way the thermal behavior of the system is closely related with delocalization[35, 36]. Thus, thanks to its simplicity the Dicke model opens a door for the study of equilibrium and thermalization in isolated quantum many-body systems, as well as for the classical-quantum correspondence issue.

In this comment we present a description of recent methods developed by our group to gauge the presence of chaos in quantum systems described by algebraic Hamiltonians. The qualitative description of regularity and chaos in the Dicke model has been performed employing Poincaré sections for the classical analysis and Peres Lattices in the quantum case. They have been discussed in our previous comment [37]. Also, in this contribution we review the study of the classical dynamics employing Lyapunov exponents as presented in [39], as well as its comparison with the quantum

Participation Ratio discussed in [38], providing a self-contained introduction to the subject, and including new results which strengthen the conclusion that, in algebraic systems, the quantum Participation Ratio (PR) of coherent states on the eigenenergy basis plays a role equivalent to the Lyapunov exponent.

The article is organized as follows. In section 2 we describe the Dicke Hamiltonian and its classical limit. In section 3 we employ the Participation Ratio of coherent states in order to quantify chaos in phase space using the eigenstates of the Dicke Hamiltonian. Finally, we expose our conclusions.

2. Quantum and classical Dicke Hamiltonians

The Dicke Hamiltonian is written in terms of the operators of the Heisenberg-Weyl HW_4 and the $SU(2)$ algebras, for the boson and collective pseudospin parts, respectively. It reads (with $\hbar = 1$),

$$H_D = \omega a^\dagger a + \omega_0 J_z + \frac{2\gamma}{\sqrt{\mathcal{N}}} J_x \left(a + a^\dagger\right). \tag{1}$$

The $a^\dagger$ and a are the creation and annihilation operators of the boson field, J_z, J_x, J_y are collective atomic pseudo-spin operators, and $j(j+1)$ is the eigenvalue of $\mathbf{J}^2 = J_x^2 + J_y^2 + J_z^2$, where j is the pseudospin length. The parameters of the Hamiltonian are ω, ω_0, and γ, which correspond to the boson frequency, the two-level energy split, and the coupling between the boson and the pseudospin. In addition, the Hamiltonian has two symmetries. First, it commutes with the $\mathbf{J^2}$ operator which divides the Hilbert space into subspaces with fixed j. In the last years the study of the Hamiltonian properties has been restricted to the subspace $j = \mathcal{N}/2$ because it corresponds to the maximum value of the pseudospin length and defines the symmetric atomic subspace which includes the ground state of the whole system. The second one is the parity operator $\Pi = e^{i\pi\Lambda}$, with $\Lambda = a^\dagger a + J_z + j$. The eigenvalues $\lambda = n + m + j$ of the Λ operator are the total number of excitations, where n is the number of photons and $n_{exc} = m + j$ the number of excited atoms. As the Hamiltonian commutes with the parity operator, its eigenstates have one of the two different parities. In spite of having the parity as a conserved quantity, the Hamiltonian has not enough conserved quantities as degrees of freedom to label every single eigenstate with a complete set of commuting operators quantum numbers. In this sense, the Dicke Hamiltonian is non-integrable, ant thus, it presents quantum chaos signatures. On the other hand, within the rotating-wave approximation (RWA) the Dicke model becomes the Tavis-Cummings model [40], which commutes with Λ, making itself integrable.

2.1. Classical Hamiltonian

By employing the coherent states of the HW_4 and $SU(2)$ algebra, i.e., Glauber and Bloch coherent states, it is possible to obtain an effective classical Hamiltonian. Being not the only way to get the correspondent classical Hamiltonian [41]. However, the classical Dicke Hamiltonian obtained via these coherent state representation, has been studied before [42] and it has been proved very useful for our ends so far [43, 44, 51, 37, 38, 39]. The validity of the use of coherent states is under the assumption the system remains in the coherent state product during the temporal evolution, so its dynamical properties are described mainly by it [45]. Alternatively, the classical Hamiltonian obtained by considering the expectation value of the Dicke

Hamiltonian in the coherent state product, is the resulting lowest order semiclassical approximation to the quantum propagator written in terms of coherent sates [46].

We calculate the expectation value of the Hamiltonian in the coherent state product $|\alpha\rangle \otimes |z\rangle$ of Glauber and Bloch coherent states [42], defined as,

$$|\alpha\rangle = e^{-|\alpha|^2/2} e^{\alpha a^\dagger} |0\rangle, \tag{2}$$

$$|z\rangle = \frac{1}{\left(1+|z|^2\right)^j} e^{zJ_+} |j,-j\rangle. \tag{3}$$

A classical description with canonical variables is obtained from the complex parameters α and z defining $\alpha = \sqrt{\frac{j}{2}}(q+ip)$ with q and p reals, and the stereographic projection of $z = \tan(\theta/2)e^{i\phi}$, from which we define $\tilde{j_z} = (j_z/j) = -\cos\theta$ and $\phi = \arctan(j_y/j_x)$, where θ and ϕ are spherical angular variables of a classical vector $\vec{j} = (j_x, j_y, j_z)$ with $|\vec{j}| = j$, and θ measured respect to the negative z-axis. The classical Hamiltonian per particle reads,

$$h_{cl}(p,q,\tilde{j_z},\phi) = \frac{\langle \alpha, z|H_D|\alpha, z\rangle}{j} = \tag{4}$$

$$= \omega_0 \tilde{j_z} + \frac{\omega}{2}\left(q^2+p^2\right) + 2\gamma\sqrt{1-\tilde{j_z}^2}\, q\, \cos\phi, \tag{5}$$

with classical equations of motion given by

$$dq/dt = \partial h_{cl}/\partial p \qquad dp/dt = -\partial h_{cl}/\partial q$$

$$d\phi = \partial h_{cl}/\partial \tilde{j}_z \qquad d\tilde{j}_z/dt = -\partial h_{cl}/\partial \phi.$$

2.2. Parameters Space and QPT

As mentioned before, the Dicke Hamiltonian presents Quantum Phase Transitions (QPT), both in the ground-state and in the spectrum, the so-called Excited-State Quantum Phase Transitions. The ground-state QPT has been motive of great interest along the years. It describes the transition from a normal to a superradiant phase, and has been classified as a second order phase transition in thermodynamical sense [23, 24, 25, 26]. When temperature goes to zero, the singular behavior remains [47], so when the coupling reaches a critical value $\gamma_c = \sqrt{\omega\omega_0}/2$ a macroscopic population of the upper atomic level takes place where the number of photons and excited atoms scales with $\mathcal{N}$, i.e. a superradiant state appears in the ground state of the system. This separates the parameter space in two parts: the normal phase ($\gamma < \gamma_c$), with no photons and no excited atoms, and the superradiant phase ($\gamma > \gamma_c$). Given that the number of bosons is unbounded, the range of energies $\epsilon = E/j$ is only lower bounded. Then, the second-order QPT appears as a discontinuity on the second derivate of the ground-state energy $\epsilon_0(\gamma)$. It can be calculated semi-classically [43, 48, 62], and it can be expressed as

$$\epsilon_0(\gamma) = \begin{cases} -\omega_0 & \text{for } \gamma \leq \gamma_c, \\ -\frac{\omega_0}{2}\left(\frac{\gamma_c^2}{\gamma^2} + \frac{\gamma^2}{\gamma_c^2}\right) & \text{for } \gamma > \gamma_c. \end{cases} \tag{6}$$

On the other hand, as we go up in energy in the superradiant region, the energy surface of the semiclassical Hamiltonian takes different structures in connection with changes in the available phase space. These changes are related to fixed points and produce

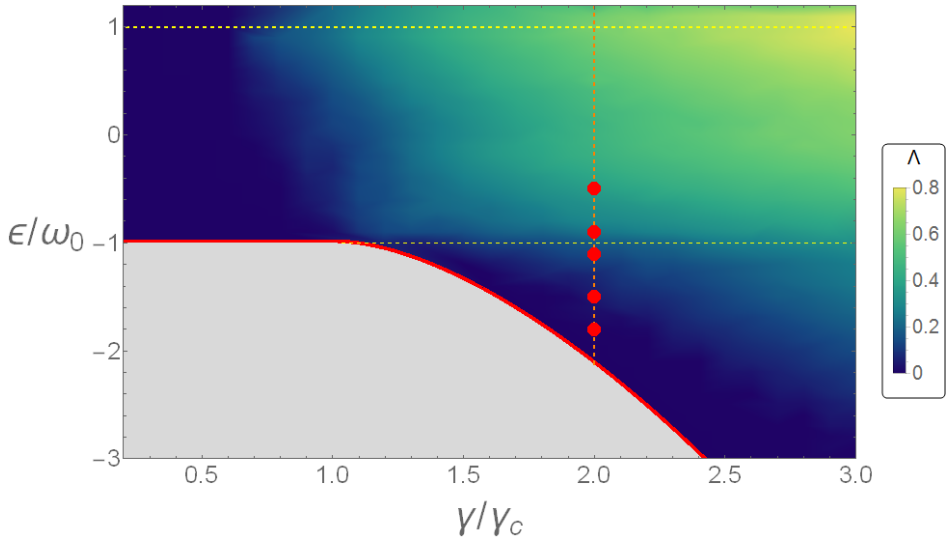

Figure 1. Averaged Lyapunov exponent over constant energy shells in the energy-coupling space, for resonance $\omega = \omega_0 = 1$. The red points indicate the cases where the P_R is compared against the Lyapunov exponent. These cases have the coupling $\gamma = 2.0\gamma_c$ and energies $E/(j\omega_0) = \epsilon/\omega_0 = -1.8, -1.5, -1.1, -0.9$ and -0.5. Thick red line indicates the ground-state energy, whereas the dashed horizontal lines signal the ESQPT energies at $\epsilon/\omega_o = -1$ and 1.

singularities in the slope of the quantum density of states (DoS), called Excited-State Quantum Phase Transitions (ESQPT) [32, 33, 34, 37, 38, 49, 50, 51, 52, 53]. While the QPT separates the parameter space of the Hamiltonian in two phases, the ESQPT separates the energy-parameter space into three regions. In the interval $\epsilon \in [\epsilon_0(\gamma), -\omega_0]$, the classical surface of constant energy is formed by two disconnected lobes (see top row of Fig.2). At $\epsilon = -\omega_0$ both lobes get connected indicating the first ESQPT, which we have called *dynamical* as it is only present in the superradiant phase, i.e. it depends on the parameters of the Hamiltonian. The second energy region is in the interval $\epsilon \in [-\omega_0, +\omega_0]$. There, the energy surface corresponds to a single lobe restricted to a limited region inside the Bloch sphere (see bottom row of Fig.2). Finally, a third region appears for energies greater than ω_0. Here, the entire Bloch sphere is available, saturating the atomic phase space. The last two regions exist in both the normal and superradiant phases and they are separated by a second ESQPT which remains independent of the coupling, so we called it *static* [37, 38, 50, 51]. The Dicke Hamiltonian is also very interesting because it possess regions with mixed regularity and chaos. At first, it was thought the ESQPT was connected with the onset of chaos. However, recent works have shown that chaos and ESQPTs are two distinct phenomena whose relation depends on the system [33, 34, 39]. A map of chaos and regularity can be done by calculating the averaged Lyapunov exponent over constant energy shells in the energy-parameter space. This map gives us insight about the chaotic behavior of the Hamiltonian and how it is related with the quantum version [39]. In figure 1 we show this map, as well as the five points where we are going to compare the Lyapunov exponent with the quantum measure of classical chaos we propose.

The Lyapunov exponents are asymptotic measures characterizing the average rate of growth (or shrinking) of small perturbations along the solutions of a dynamical system. In regular, nonchaotic systems, the distance between a given trajectory and another one, built from a small perturbation in the initial conditions, remains close to zero, or increases at most algebraically as time evolves. In chaotic systems this distance diverges exponentially in time. The Lyapunov exponent characterizes this instability along the path. When it is positive, the trajectory is extremely sensible to the initial condition and is called chaotic. Details of the calculation can be found in the Appendix A of Ref. [39]. In Fig. 1 the dark blue areas are regular, while the light green ones are chaotic. It is important to emphasize that this map of chaos and regularity is a very important guide for the study of the correspondence between the classical and the quantum system. Also, we expect it would be helpful to explore the equilibration and thermalization issues in the Dicke model, having it as a reference of chaotic behavior for the quantum model.

3. Participation Ratio as a quantum measure of chaos

In the context of the kicked top, in [12] F. Haake proposed that the minimum number of eigenstates of the Floquet operator necessary to reconstruct a coherent state, D_{min}, could be used to identify chaotic and regular regimes. It was also shown that the D_{min} scales with the size, L, of the system as $\sqrt{L}$ in regular regions and as L in chaotic ones. The proposal depends on the idea of localization. In the regular regions, the coherent state tends to be localized around few states, in correspondence with the classical regular movement while a coherent state associated with a chaotic region would be delocalized. Therefore, in the thermodynamical limit $L \to \infty$, an infinitely small fraction of eigenstates ($\sqrt{L}/L = 1/\sqrt{L}$) would be enough to reconstruct a coherent state associated with regular regions, however, this fraction goes to a finite value in the chaotic region. It was also suggested that this measure is an analogue of the classical Lyapunov exponent. Inspired by this idea we employ the Participation Ratio of a coherent state spanned in the Hamiltonian eigenstate basis. Each coherent state correlates with one point in the classical phase space of the classical Dicke Hamiltonian, and in our context the number of atoms j is the relevant dimension of the system, directly associated with the eigenstate basis.

As mentioned before, we use the Participation Ratio P_R as a measure of localization of the quantum state. It was introduced several years ago in the context of solid state physics, the Quantum Hall effect and Anderson localization [54, 55, 56, 57, 58]. For the Dicke model it has been employed in the study of the equilibrium [59]. Also, it has been used to show that the equilibration process depends on the spreading of the initial state over the perturbed basis [60]. The main advantage over the D_{min} criterion is that the P_R does not requieres a cutoff (the smallest relevant contribution), which could be arbitrary. The P_R as a measure of localization has its own scale because it is normalized. That this localization in the space of eigenstates effectively takes place in the Dicke model can be seen in the distribution of the coherent state over the Hamiltonian eigenbasis, as shown in Fig. 3 and 4 of Ref. [38]

For a pure quantum state $|\Psi\rangle$, expanded in a N-dimensional basis $\{|\phi_k\rangle\}$, the participation ratio is

$$P_R = \frac{1}{\sum_{k=1}^{N} |\langle\phi_k|\Psi\rangle|^4}. \tag{7}$$

The participation ratio is defined in the interval $P_R \in [1, N]$. When $P_R = 1$ it means the state $|\Psi\rangle$ is identical to one of the states of the basis, and it is considered as having maximum localization. On the other hand, if every state of the basis equally contribute to the state, we would have $|\langle\phi_n|\Psi\rangle| = 1/\sqrt{N}$. In this case $P_R = N$. So, the maximum value of the P_R is related to maximum delocalization in the Hilbert space.

The P_R of the coherent state $|\alpha_0, z_0\rangle$, which identifies a point in the classical phase-space, over the Hamiltonian eigenstates, $|E_k\rangle$, is

$$P_R = \frac{1}{\sum_k |\langle E_k|\alpha_0, z_0\rangle|^4} = \frac{1}{\sum_k Q_k^2(\alpha_0, z_0)}, \tag{8}$$

where $Q_k^2(\alpha_0, z_0)$ is the Husimi function of the $k-th$ eigenstate $|E_k\rangle$ of the Dicke Hamiltonian. The Husimi or Q function, $Q_k(\alpha, z) = |\langle z, \alpha|E_k\rangle|^2$, is one of the simplest distributions of quasiprobability in phase space. It has a well-defined classical limit and allows to study the classical-quantum correspondence [45]. Also, in the thermodynamical limit it reduces to a classical probability function on phase space obeying the Liouville equation [5]. The Husimi function has been employed in the Dicke model by several authors to study the quantum-classical transition and equilibration [5, 45], the wave functions of individual states [42, 45], and the ground-state QPT [61, 63].

In order to better compare the quantum results (based on the P_R) with the classical ones (based on the Lyapunov exponent), we define binary quantities. We consider the quantity $P_R/\mathcal{N}$, and we assign $P_{Rbin} = 0$ when $P_R/\mathcal{N} < 1$ and $P_{Rbin} = 1$ when $P_R/\mathcal{N} > 1$. This binary quantity gives a very simple criterion allowing to distinguish roughly when the participation ratio scales slower than the number of atoms. Analogously, for the Lyapunov exponent we define Λ_{bin} as $\Lambda_{bin} = 0$ if $\Lambda < 0.002$ and $\Lambda_{bin} = 1$ if $\Lambda > 0.002$. The numerical tolerance $\Lambda_T = 0.002$ employed to distinguish a chaotic from a regular classical trajectory, is rooted in the numerical precision employed in solving the equations of motion. Both binary criteria are somewhat arbitrary, and care has to be taken when the respective values, $P_R/\mathcal{N}$ and Λ, are close to the tolerance limits employed (1 and 0.002 respectively). In the following we are going to explore these quantities along the energy surfaces.

3.1. The efficient coherent basis

In the evaluation of the Participation Ratio P_R the challenge is to obtain the exact quantum eigenstates $|E_k\rangle$ of the Dicke Hamiltonian. Being the Hamiltonian non-integrable, the solutions (to obtain the spectrum and the eigenfunctions) must be numerical. On the other hand, given that the Hilbert space is infinite, the numerical calculations must be performed in a truncated space, and the convergence of each one of the eigenstates which are relevant in the expansion of a coherent state must be guaranteed. To perform this task we employ the efficient coherent basis (ECB), which is the exact Hamiltonian eigenbasis in the limit $\omega_0 = 0$ [64, 65].

The ECB is built from vacuum sates, $|0\rangle_{m_x}$, defining new bosonic displaced operators $A = a + \frac{2\gamma}{\omega\sqrt{\mathcal{N}}} J_x$,

$$|N; j, m_x\rangle = \frac{(A^\dagger)^N}{\sqrt{N!}}|0\rangle_{m_x}. \tag{9}$$

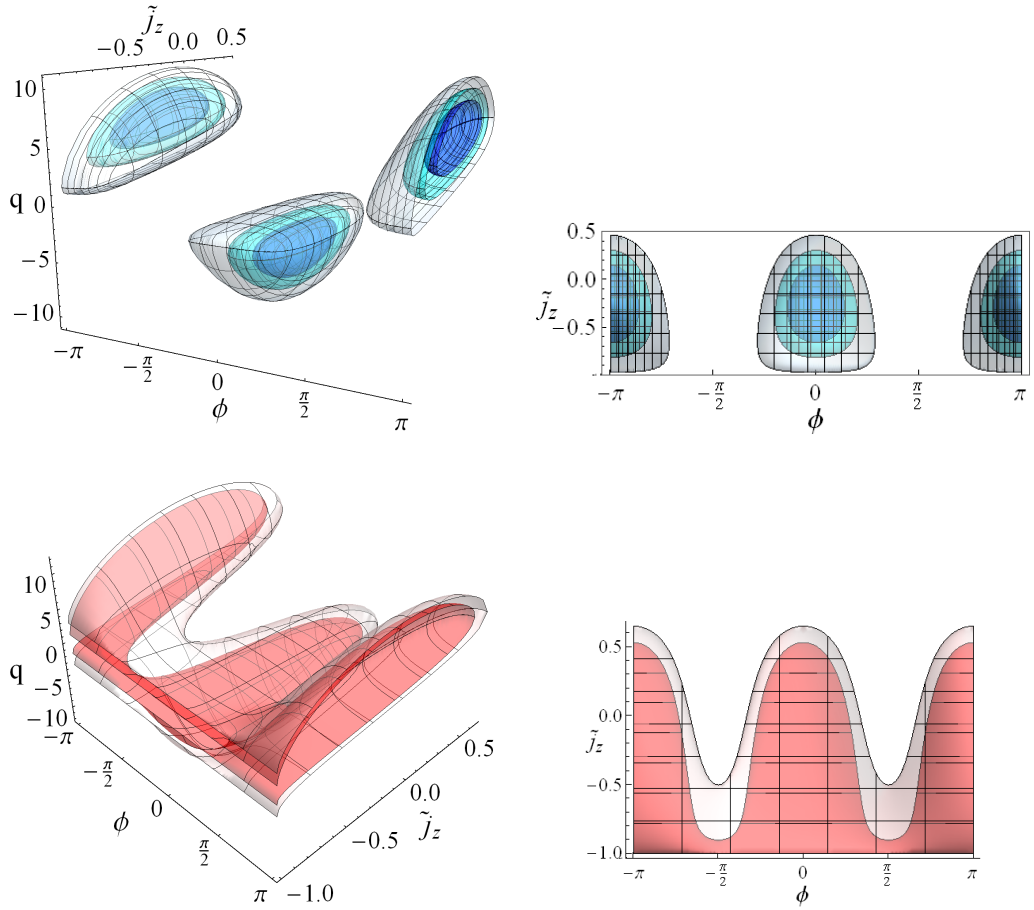

Figure 2. Left column: Poincaré surfaces ($p = 0$) for the energies indicated in Fig.1. Top panel shows the surfaces for energies below the ESQPT, from the inner to the outer surface these energies are, respectively, $\epsilon/\omega_o = -1.8, -1.5$ and -1.1. Bottom panel is for energies above the ESQPT, $\epsilon/\omega_o = -0.9$ and -0.5 for the inner and outer surface respectively. Every surface is formed by an upper and lower shell, q_+ and q_-, given by the solutions shown in Eq.(10). Right column shows the projection of the Poincaré surfaces in the $(\tilde{j_z}, \phi)$ plane.

These vacuum states are obtained from rotated (by $-\frac{\pi}{2}$ around the y-axis) atomic states, eigenstates $|j, m_x\rangle$ of J_x

$$|0\rangle_{m_x} = |\alpha_{m_x}\rangle|j, m_x\rangle,$$

where $|\alpha_{m_x}\rangle$ is a boson coherent state with Glauber parameter $\alpha_{m_x} = -2\gamma m_x/(\omega\sqrt{\mathcal{N}})$, which guarantees that $A|0\rangle_{m_x} = 0$.

The benefits of employing this particular basis are notorious. It allows to obtain a number of converged eigenstates orders of magnitude larger than that which can be obtained with the same cut-off in the standard Fock basis, based in the number of photons and the eigenstates of J_z. It is particularly useful in the study of large systems in the superradiant phase, which rapidly become numerically intractable in the Fock basis [65, 66, 67]. Details and explicit expressions for the evaluation of the

Husimi function, and for the Participation Ratio, in the efficient coherent basis are given in Appendix C of Ref. [38].

4. Participation Ratio over different energy sections

We present results for different energies with a single value of the coupling. They are shown as red dots in Fig. 1. We have selected the superradiant phase with $\gamma = 2.0\,\gamma_c$ in resonance $\omega = \omega_0 = 1$, as the correspondent classical Hamiltonian of the Dicke model shows different mixings of chaos and regularity, from a complete region of regularity at low energies, to full ergodic chaos [39].

To choose the classical canonical coordinates which define each coherent state, we consider classical Poincaré surfaces of given energy, fixing $p = 0$. Then we find the variables ϕ, $\tilde{j_z}$, and q satisfying $H_{cl}(q, p = 0, \tilde{j_z}, \phi) = \epsilon$. The choice $p = 0$ ensures a broad sampling of the classical orbits because all of them intersects these Poincaré energy surfaces. Under these conditions, we have two different values of q,

$$q_{\pm}(\tilde{j_z}, \phi, \epsilon) = -\frac{2\gamma}{\omega}\sqrt{1-\tilde{j_z}^2}\,\cos\phi \pm \sqrt{\frac{4\gamma^2}{\omega^2}\left(1-\tilde{j_z}^2\right)\cos^2\phi + \frac{2}{\omega}\left(\epsilon - \omega_0\tilde{j_z}\right)}. \tag{10}$$

By choosing the energy ϵ, and single values of $\tilde{j_z}$ and ϕ we have a single point in the phase space identified unambiguously within each of the surfaces $q_{\pm}$. The Poincaré surfaces for the selected energies in this study are shown in Fig.2.

With these elements we define coherent states $|\alpha, z\rangle$ with $\alpha = \sqrt{\frac{j}{2}}q_{\pm}\left(\epsilon, \tilde{j}_z, \phi\right)$ and $z = \sqrt{\frac{1+\tilde{j}_z}{1-\tilde{j}_z}}e^{i\phi}$. The same Poincaré surfaces are used to obtain Poincaré sections of the classical model, which provide a qualitative insight of the presence of chaos [9, 11, 37]. Projections of these Poincaré sections in the plane $\tilde{j}_z$-ϕ, are shown in Fig.3 for the five energies shown with red dots in Fig. 1, and for both energy surfaces q_+ (left) and q_- (right).

In the following we present a detailed comparison between the P_R as a quantum measure of chaos and the Lyapunov exponent. Due to the numerical effort in calculating the P_R, we restrict ourselves to the line with $\phi = 0$, for each of the $q = q_+$ and $q = q_-$ surfaces, for the five representative energies: $\epsilon = -1.8\omega_0$, $\epsilon = -1.5\omega_0$, $\epsilon = -1.1\omega_0$, $\epsilon = -0.9\omega_0$, and $\epsilon = -0.5\omega_0$. All the calculations are done with the Hamiltonian parameters $\gamma = 2.0\gamma_c$ and $\omega = \omega_0 = 1$. The number of atoms is fixed to $\mathcal{N} = 160$ ($j = 80$). In the binary case, as both Λ_{bin} and P_{Rbin} are zero or one, they are slightly displaced vertically for better visualization.

4.1. Regular region $\epsilon = -1.8$

For the set of parameters chosen, the ground-state energy is $\epsilon_{g.s.} = -2.125$. Then, around the value $\epsilon = -1.8$ we expect to have regular behavior.This is confirmed qualitatively by the regular orbits in the Poincaré section as can be observed in the uppermost panels of figure 3. The presence of low energy regular regions can be understood by the existence of approximate integrals of motion, associated with the decoupling of the two collective degrees of freedom of the system [68].

In this case both the Lyapunov exponent and the Participation Ratio (compared with the number of atoms) are pretty small, fully confirming that the region is regular. In the binary case, Fig. 4 bottom, both quantities are null. The P_R predicts the regularity of every point at the same extent as the Lyapunov exponent.

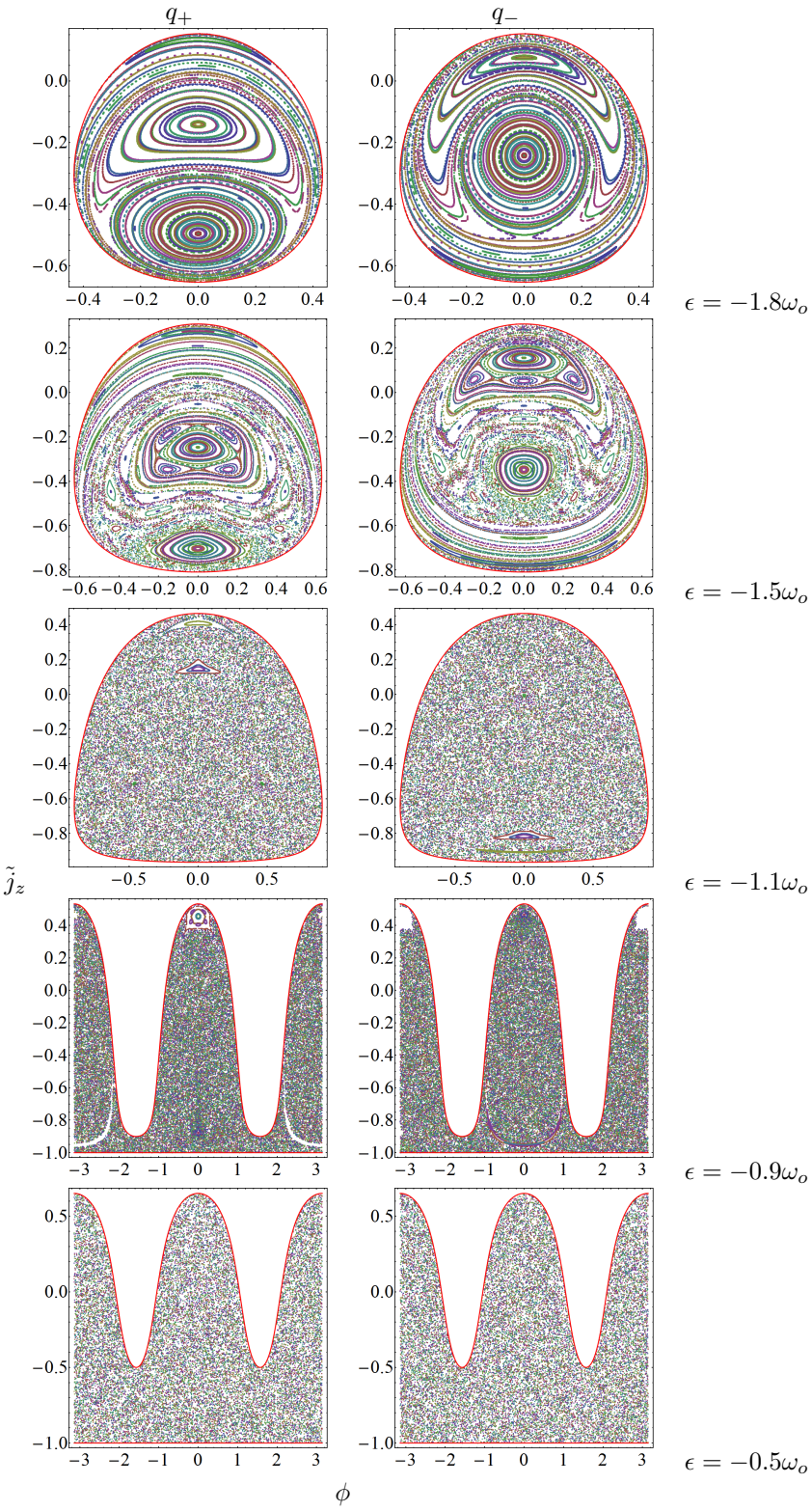

Figure 3. Poincaré sections ($p = 0$) projected over the $\tilde{j}_z$-ϕ plane, for the energies indicated in Fig.1. Left and right columns correspond, respectively, to the projections of the q_+ and q_- shells of the Poincaré surface.

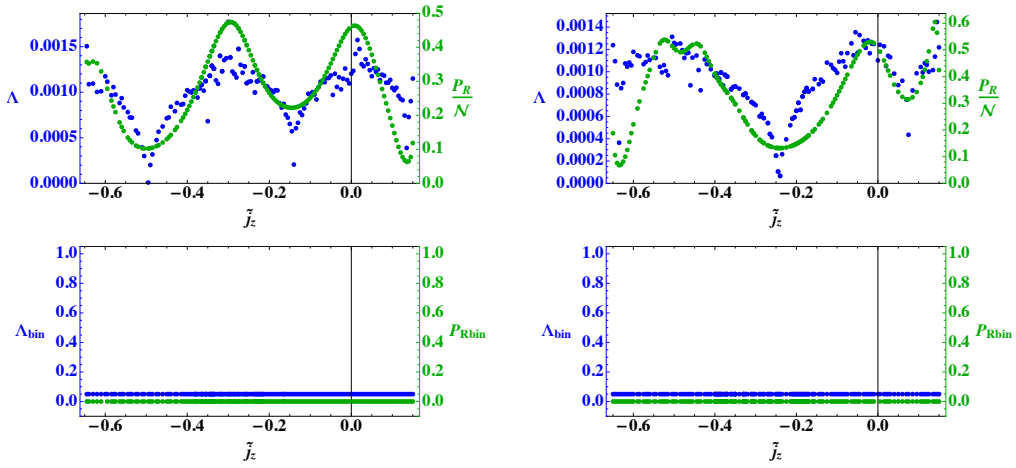

Figure 4. Energy $\epsilon = -1.8$. Top: Participation Ratio (green) and Lyapunov exponent (blue) for the q_+ surface (left) and q_- surface (right) and their binary versions (bottom).

It must be noted that the maximal Lyapunov and $P_R/\mathcal{N}$ obtained in this case, are close to the tolerance cuts used to distinguish regularity from chaos. Therefore, as mentioned before, a more carefully analysis has to be done in these cases to establish unambiguously the presence of chaos. A particular example of this situation is discussed at the end of this section, where the scaling of the Participation Ration with the number of atoms is studied.

4.2. Mixed region $\epsilon = -1.5$

Moving up in energy to $\epsilon = -1.5$ we observe in phase space that regularity and chaos coexist as it could be seen from Fig. 3. In Fig. 5 there are three small but visible regions for each set of $q's$ where both the Lyapunov exponent and the Participation Ratio announce the presence of chaos. For q_+, Fig. 5 left, they are around $\tilde{j_z}$ -0.8, -0.6 and 0.0. For q_-, Fig. 5 right, they are around $\tilde{j_z}$ -0.6, -0.1 and 0.3. This is the most important point which we are communicating in this Comment: *the quantum Participation Ratio (PR) of coherent states on the eigenenergy basis plays a role equivalent to the Lyapunov exponent.* The support of this affirmation can be found in the figures of the present section.

We are aware that the agreement between the regions in phase space described as chaotic employing the classical Lyapunov exponent and the quantum Participation Ratio is not perfect. The differences are originated by two limitations. One is the incertitude in the value of the tolerance cut which delimits regularity from chaos in the numerical studies, as mentioned in the previous section. The second one is that the Participation Ration becomes a better identifier of the presence of chaos as the number of atoms included in the calculation increases, but the numerical implementation can easily become prohibitive.

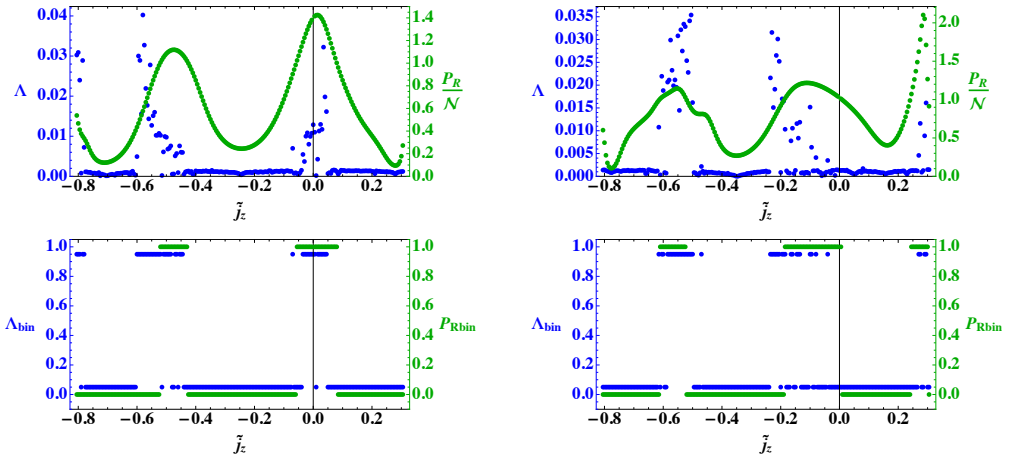

Figure 5. Energy $\epsilon = -1.5$. Top: Participation Ratio (green) and Lyapunov exponent (blue) for the q_+ surface (left) and q_- surface (right) and their binary versions (bottom).

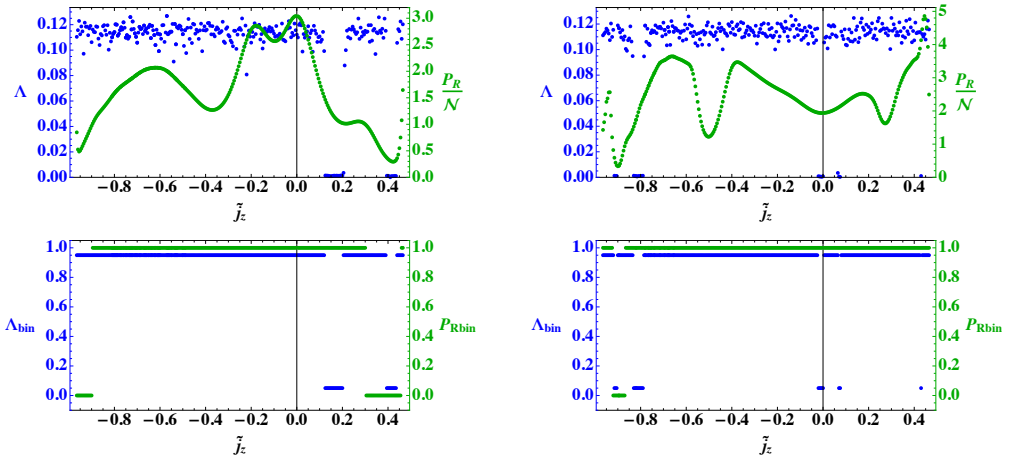

Figure 6. Energy $\epsilon = -1.1$. Top: Participation Ratio (green) and Lyapunov exponent (blue) for the q_+ surface (left) and q_- surface (right) and their binary versions (bottom).

4.3. Just below the ESQPT region $\epsilon = -1.1$

Moving upper in energy, at $\epsilon = -1.1$ we approach the ESQPT from below. In this case in phase space we observe that the system is mostly chaotic, with some small islands of regularity. In Fig. 6 there are regions for each set of $q's$ where both the Lyapunov exponent and the Participation Ratio are still very small. For q_+, Fig. 6 left, these regions are around $\tilde{j_z}$ -0.9, 0.2 and 0.4. For q_-, Fig. 6 right, they are around $\tilde{j_z}$ -0.9 and 0.0. Both the Lyapunov exponent and the Participation Ratio detect these regions, with the limitations mentioned above.

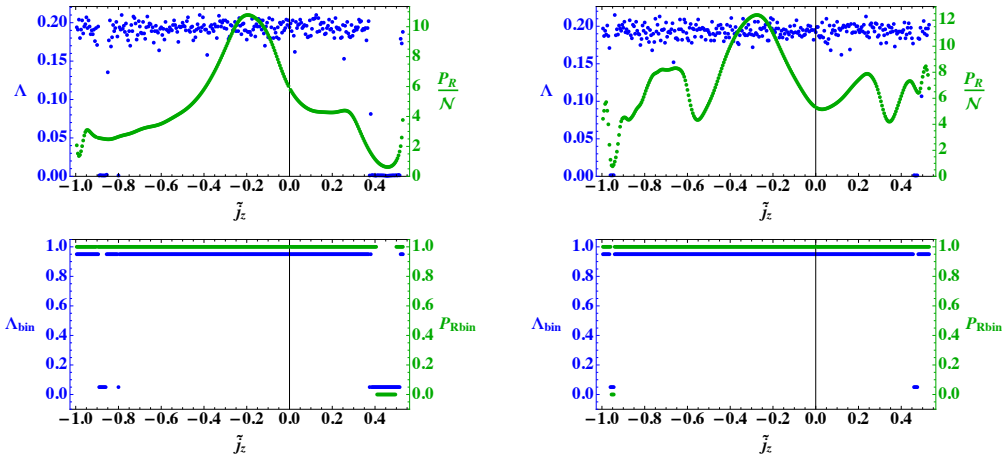

Figure 7. Energy $\epsilon = -0.9$. Top: Participation Ratio (green) and Lyapunov exponent (blue) for the q_+ surface (left) and q_- surface (right) and their binary versions (bottom).

4.4. Just above the ESQPT region $\epsilon = -0.9$

For an energy $\epsilon = -0.9$ we are located just above the ESQPT. As in the previous case, the system is almost fully chaotic, with some small islands of regularity. In Fig. 7 there are just a couple of regions for each set of $q's$ where both the Lyapunov exponent and the Participation Ratio are close to zero. For q_+, Fig. 7 left, that couple is around $\tilde{j}_z$ -0.9 and 0.4. For q_-, Fig. 7 right, that is around $\tilde{j}_z$ -1.0 and 0.5. Again, both the Lyapunov exponent and the Participation Ratio detect these regions.

4.5. Fully chaotic region $\epsilon = -0.5$

At energy $\epsilon = -0.5$ the phase space is fully chaotic. In Fig. 8 both the Lyapunov exponent and the Participation Ratio have values far larger than their numerical tolerance cuts. The comparison between them is straightforward, as it was for the regular cases at low energies. Both criteria indicates the phase space is completely chaotic.

As mentioned above, in all cases we observe a very good global agreement between the P_R and the Lyapunov exponent. The global agreement is better seen in the case of the binary criterion. The differences which remain can be attributed to the finite value of j. In the thermodynamical limit we expect the Lyapunov and the P_R binary quantities will perfectly match.

4.6. Scaling of the P_R

We have already exhibited that the behavior of the classical Lyapunov exponent and the quantum Participation Ratio follows each other, they are both large in chaotic regions and small in the regular ones. We have also corroborated that the limits for the binary quantities, $\Lambda_{bin} = 0$ if $\Lambda \leq 0.002$ and $P_{Rbin} = 0$ if $P_R \leq \mathcal{N}$, define a numerical criteria to distinguish regularity or chaos. Close to these limits the system is in the

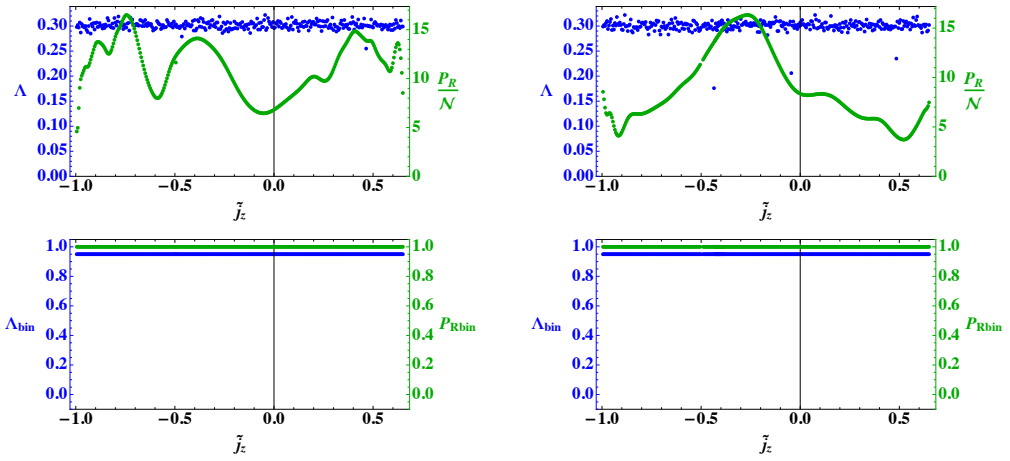

Figure 8. Energy $\epsilon = -0.5$. Top: Participation Ratio (green) and Lyapunov exponent (blue) for the q_+ surface (left) and q_- surface (right) and their binary versions (bottom).

route to chaos, making it numerically difficult to distinguish regularity and chaos, a factor of order two could easily modify these limits without changing noticeably neither the above analysis nor their conclusions.

In Ref. [38] we advanced an additional quantitative criteria which can be used to determine if a particular point in phase space is associated with a regular or chaotic dynamics employing the Participation Ratio of coherent state on the Hamiltonian eigenstate basis. It involves the numerically more demanding task of evaluating the P_R as a function of $\mathcal{N} = 2j$, and analyzing its functional dependence. If $\lim_{j\to\infty} P_R/\mathcal{N}$ goes to zero, we can confidently conclude that this coherent state is localized in the eigenstate basis in the thermodynamic limit, and the associated classical trajectory is regular. If this condition is not fulfilled, this point in phase space has a chaotic dynamics.

In Fig 9 we show the scaling of some specific points which belong to the energy surfaces explored above. We have selected two points in phase space for three energies, $\epsilon = -0.5$ (left), $\epsilon = -1.5$ (center), and $\epsilon = -1.8$ (right). The selected points in each case correspond to those with the largest (blue) and smallest (red) Lyapunov exponent in the q_+ branch of the energy surface. They are listed in Table 1, where the values of the energy ϵ, the pseudospin coordinate $\tilde{j}_z$, the Lyapunov exponent Λ and the function providing a fit of the data are given. The fitting functions are representative of the asymptotic behaviour of the Participation Ratios for large number of atoms. They scale as $P_r \propto N^\alpha$ with $\alpha \approx 1/2$ for regular points and as $P_r \propto N^\alpha$ with $\alpha \gtrsim 1$ for chaotic ones.

At the highest energy $\epsilon = -0.5$, Fig. 9 (left), it can be seen how the Participation Ratio grows faster than the number of atoms, revealing both points as chaotic, in correspondence with the Lyapunov exponent which is much larger than 0.002 for both points. At the intermediate energy $\epsilon = -1.5$, Fig. 9 (center), the Participation Ratio associated with the largest Lyapunov exponent (much greater than 0.002) shown as blue points, grows faster than the number of atoms and is identified also as chaotic.

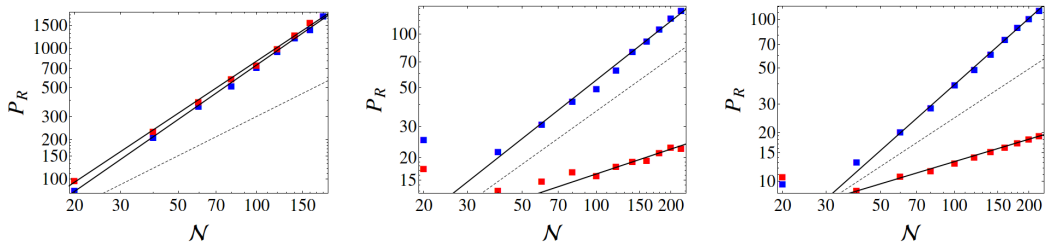

Figure 9. The Participation Ratio P_R as a function of the number of atoms $\mathcal{N}$ in log-log scale, for three different energies $\epsilon = -0.5$ (left), $\epsilon = -1.5$ (center), and $\epsilon = -1.8$ (right). The blue (red) dots represent the values for the points ($\phi = 0$, $\tilde{j}_z$, $p = 0$ and q_+) with the largest (smallest) Lyapunov exponent in left panels of Figs.4, 5 and 8. The continuos lines correspond to the fits listed in Table 1. The dashed lines show the slope of a linear dependence $\propto N$, giving a guide to distinguish between scalings faster or slower than the number of atoms.

ϵ	$\tilde{j}_z$	Λ	Fit
-0.5	-0.435	0.176	$P_R = 1.76N^{1.328}$
-0.5	0.075	0.322	$P_R = 1.26N^{1.386}$
-1.5	-0.300	0.00014	$P_R = 0.640N^{0.466}$
-1.5	-0.580	0.040	$P_R = 0.34N^{1.103}$
-1.8	-0.495	9.18×10^{-6}	$P_R = 1.61N^{0.458}$
-1.8	-0.705	0.0018	$P_R = 0.08N^{1.354}$

Table 1. The six points in phase phase for which the scaling of the Participation Ratio with the number of atoms is plotted in Fig. 9.

On the other hand, the red dots, representing the Participation Ratio of the point with the smallest Lyapunov exponent (much smaller than 0.002), scales much slower than $\mathcal{N}$, allowing its identification as a regular point in phase space. At the low energy $\epsilon = -1.8$, Fig. 9 (right), a pattern similar to the one described for the intermediate energy occurs. For the point with the smallest Lyapunov exponent (much smaller than the tolerance 0.002), we find, as expected, a scaling $P_R \propto N^{1/2}$. What came somehow as a surprise is that the Participation Ratio of the point with the largest Lyapunov exponent, scales faster than $\mathcal{N}$ and seems to be chaotic. This can be understood because in this point $\Lambda = 0.0018$, which is very close to the limit of 0.002 established to separate regular from chaotic dynamics. This case exhibits the dependence of P_R on $\mathcal{N}$ as a very sensitive test, which is able to identify chaotic points in a phase space which is almost 100% regular (see uppermost panels of Fig.3).

5. Conclusions

In this contribution we have exhibited the Participation Ratio (PR) of coherent states on the eigenenergy basis as a purely quantum tool to identify the regular and chaotic regions in phase space for systems which have an algebraic Hamiltonian, in the particular case of the Dicke Hamiltonian. It requires the introduction of coherent states, which provides the bridge connecting the quantum and classical realms. This work goes far beyond the qualitative analysis based in Poincaré sections and Peres lattices presented in [37], explotes quantitatively the semiclassical study on chaos in

the Dicke model discussed in [39], and extends the results discussed in [38].

As the non-integrable Dicke model has regions associated with regular and chaotic motion, we have quantitatively evaluated the presence of classical chaos employing the largest Lyapunov exponent in the whole available phase space for a given energy. In the quantum regime, the use of very efficient diagonalization techniques played a key role allowing the numerical evaluation of the quantum Participation Ratio P_R of coherent states on the eigenenergy basis. We have shown that it plays a role equivalent to the Lyapunov exponent. We have also shown that, in the thermodynamic limit, the quotient of the Participation Ratio and the number of atoms goes to zero in the regular regions and tends to a positive value in the chaotic ones, thus allowing us to define a criterion to identify chaos employing only quantum concepts.

The present proposal can be applied to any quantum mechanical system when it is possible to build a classical phase space through a semiclassical treatment, and it can be useful for other algebraic non-integrable models.

Acknowledgments

We acknowledge financial support from Mexican CONACyT projects CB166302, CB2015-01/255702 and DGAPA-UNAM project IN109417. S.L-H. acknowledges financial support from the CONACyT fellowship program for sabbatical leaves.

References

[1] A. Polkovnikiv, K. Sengupta, A. Silva, M. Vengalattore, *Rev. Mod. Phys.* **83**, 863 (2011).
[2] J. Eisert, M. Friesdorf, and C. Gogolin, *Nature Physics* **11**, 124 (2015).
[3] C. Gogolin and J. Eisert *Rep. Prog. Phys.* **79** 056001 (2016).
[4] L. D' Alessio, Y. Kafri, A. Polkovnikov, and M. Rigol, it Advances in Physics **65**, 239 (2016).
[5] A. Altland and F. Haake, *Phys. Rev. Lett.* **108**, 073601 (2012); *New J. Phys.* **14**, 073011 (2012).
[6] M.V. Berry, M. Tabor, *Proc. R. Soc.Lond.*A **356**, 375 (1977).
[7] O. Bohigas, M.J.Giannoni, C.Schmit, *Phys. Rev. Lett.*, **52**, 1 (1984).
[8] M.V. Berry and M. Robnik, *J.Phys. A: Math. Gen.***17**, 2413 (1984).
[9] T. S. Parker and L. O. Chua, *Practical Numerical Algorithms for Chaotic Systems*, New York, Springer Verlag (1989).
[10] M. C. Gutzwiller, Chaos in Classical and Quantum Mechanics, Springer: New York (1990).
[11] Steven H. Strogatz, *Nonlinear Dynamics and Chaos, with applications to Physics, Biology, Chemistry and Enginnering*, Massachusetts, Perseus Books (1994).
[12] F. Haake, *Quantum Signatures of Chaos.* (Germany, Springer-Verlag, 2001).
[13] R. H. Dicke, *Phys. Rev.* **93**, 99 (1954).
[14] D. Schneble, Y. Torii, M. Boyd, E. W. Streed, D. E. Pritchard, and W. Ketterle, *Science* **300**, 475 (2003).
[15] A. Blais, R-S. Huang, A. Wallraff, S. M. Girvin, and R. J. Schoelkopf, *Phys. Rev. A* **69**, 062320 (2004).
[16] M. Scheibner, T. Schmidt, L. Worschech, A. Forchel, G. Bacher, T. Passow, and D. Hommel, *Nature Phys* **3**, 106 (2007)
[17] J. M. Fink, R. Bianchetti, M. Baur, M. G´oppl, L. Steffen, S. Filipp, P. J. Leek, A. Blais, and A. Wallraff, *Phys. Rev. Lett.* **13**, 083601 (2009).
[18] K. Baumann, C. Guerlin, F. Brennecke, and T. Esslinger, *Nature* **464**, 1301 (2010); K. Baumann, R. Mottl, F. Brennecke, and T. Esslinger, *Phys. Rev. Lett.* **107**, 140402 (2011).
[19] D. Nagy, G. Kónya, G. Szirmai, and P. Domokos, *Phys. Rev. Lett.* **104**, 130401 (2010).
[20] T. Niemczyk, F. Deppe, H. Huebl, E. P. Menzel, F. Hocke, M. J. Schwarz, J. J. Garcia-Ripoll, D. Zueco, T. Hmmer, E. Solano, A. Marx, and R. Gross, *Nat. Phys.* **6**, 772 (2010).
[21] J. Casanova, G. Romero, I. Lizuain, J. J. García-Ripoll, and E. Solano, Phys. Rev. Lett. 105, 263603 (2010).
[22] A. Mezzacampo, U. Las Heras, J. S. Pedernales, L. DiCarlo, E. Solano, and L. Lamata, *Sci. Rep.* **4**, 7482 (2014).

[23] K. Hepp and E. H. Lieb, *Ann. Phys. (N.Y.)* **76**, 360 (1973); *Phys. Rev. A* **8** (5), 2517 (1973).
[24] Y. K. Wang and F. T. Hioe, *Phys. Rev. A* **7**, 831 (1973).
[25] H. J. Carmichael, C. W. Gardiner, and D. F. Walls, *Phys. Lett.* **46 A**, 47 (1973).
[26] G. Comer Duncan, *Phys. Rev. A* **9** (1), 418 (1974).
[27] C. Emary and T. Brandes, *Phys. Rev. E* **67**, 066203 (2003); Phys. Rev. Lett. **90**, 044101 (2003).
[28] N. Lambert, C. Emary, and T. Brandes, *Phys. Rev. Lett.* **92**, 073602 (2004).
[29] J. Vidal and S. Dusuel, *Europhys. Lett.* **74**, 817 (2006)130401 (2010).
[30] P. Cejnar, M. Macek, S. Heinze, J. Jolie, and J. Dobeš, *J. Phys. A* **39**, L515 (2006).
[31] M. A. Caprio, P. Cejnar, and F. Iachello, *Ann. Phys.* **323**, 1106 (2008).
[32] P. Cejnar and P. Stránský, *Phys. Rev. E* **78**, 031130 (2008); P. Stránský, P. Hruska, and P. Cejnar, *Phys. Rev. E* **79**, 066201 (2009).
[33] P. Stránský, M. Macek, P. Cejnar, *Ann. Phys. (NY)* **345**, 73 (2014); P. Stránský, M. Macek, A. Leviatan and P. Cejnar, *Ann. Phys* **356**, 57 (2015).
[34] P. Stránský and P. Cejnar, *Phys. Lett. A* **380**, 34 (2016).
[35] E. Canovi, D. Rossini, R. Fazio, G.E. Santoro, and A. Silva, *Phys. Rev. B***83**, 094431 (2011).
[36] A. Pal, and D.A. Huse, *Phys. Rev. B***82**, 174411 (2010).
[37] M. A. Bastarrachea-Magnani, B. López-del-Carpio, S. Lerma-Hernández, and J. G. Hirsch, *Phys. Scr.* **90**, 068015 (2015).
[38] M. A. Bastarrachea-Magnani, B. López-del-Carpio, J. Chávez-Carlos, S. Lerma-Hernández, and J. G. Hirsch, *Phys. Rev. E* **93**, 022215 (2016).
[39] J. Chávez-Carlos, M. A. Bastarrachea-Magnani, S. Lerma-Hernández, and J. G. Hirsch, *Phys. Rev.* E **94**, 022209 (2016).
[40] M. Tavis and F. W. Cummings, *Phys. Rev.* **170** 379 (1968).
[41] R. Graham, and M. Z. Hhnerbach *Physik B - Condensed Matter* **57**, 233 (1984).
[42] M. A. M. de Aguiar, K. Furuya, C. H. Lewenkopff, and M. C. Nemes, *Europhys. Lett.* **15** (2), 125 (1991); *Ann. Phys.* **216**, 291 (1992).
[43] O. Castaños, E. Nahmad-Achar, R. López Peña, and J. G. Hirsch, *Phys. Rev. A* **84**, 013819 (2011).
[44] O. Castaños, E. Nahmad-Achar, R. López Peña, and J. G. Hirsch, *Phys. Rev. A* **83**, 051601 (R) (2011)
[45] L. Bakemeier, A. Alvermann, and H. Feske, *Phys Rev. A* **88**, 043835 (2013).
[46] A.D. Ribeiro, M.A.M. de Aguiar, and A.F.R. de Toledo Piza, J.Phys. A: Math. Gen. **39**, 3085 (2006).
[47] M. A. Bastarrachea-Magnani, S. Lerma-Hernández, and J. G. Hirsch, *JSTAT* **2016**, 093105 (2016).
[48] O. Castaños, E. Nahmad-Achar, R. López Peña, J. G. Hirsch, E. López Moreno and J.E. Vitela, *Phys. Scripta* **79**, 065405 (2009).
[49] P. Pérez-Ferández, A. Relaño, J. M. Arias, P. Cejnar, J. Dukelsky, and J. E. García-Ramos, *Phys. Rev. E* **83**, 046208 (2011).
[50] T. Brandes, *Phys. Rev. E* **88**, 032133 (2013).
[51] M. A. Bastarrachea-Magnani, S. Lerma-Hernández, and J. G. Hirsch, *Phys. Rev. A* **89**, 032101 (2014); *Phys. Rev. A* **89**, 032102 (2014).
[52] P. Cejnar and P. Stránský, *Phys. Scr.* **91**, 8 (2016).
[53] M. Kloc, P. Stránský and P. Cejnar, arXiv:1609.02758 (2016).
[54] R. J. Bell, P. Dean, *Discuss. Faraday-Soc.* **50**, 55 (1970).
[55] D. J. Thouless, *Phys. Rep.* **13**, 94 (1974).
[56] F. Wegner, *Z. Phys. B: Cond. Matt.* **51**, 279 (1983).
[57] S. Hikami, *Prog. Theor. Phys.* **76**, 1210 (1986).
[58] M. R. Zirnbauer, *Nuc. Phys.* **B265**, 375 (1986).
[59] I. García-Mata, A. J. Roncaglia, and D. A. Wisniacki, *Phys. Rev. E* **91**, 010902 (2015).
[60] G. Engelhardt, V. M. Bastidas, W. Kopylov, and T. Brandes, *Phys. Rev. A* **91**, 013631 (2015).
[61] E. Romera, R. del Real, and M. Calixto, *Phys. Rev. A* **85**, 053831 (2012).
[62] E. Nahmad-Achar, O. Castaños, R. López-Peña, and J. G. Hirsch. *Phys. Scr.* **87**, 038114 (2013).
[63] R. del Real, M. Calixto and E. Romera, *Phys. Scr.* **T153**, 014016 (2013).
[64] Q. H. Chen, Y. Y. Zhang, T. Liu, and K. L. Wang, *Phys. Rev. A* **78** 051801 (2008); T. Liu, Y. Y. Zhang, Q. H. Chen, and K. L. Wang, *Phys. Rev. A* **80** 023810 (2009).
[65] M. A. Bastarrachea-Magnani and J. G. Hirsch, *Rev. Mex. Fis. S* **57** 0069 (2011) http://rmf.smf.mx/pdf/rmf-s/57/3/5730069.pdf.
[66] M. A. Bastarrachea-Magnani and J. G. Hirsch, *AIP Conf. Proc.* **1488** 418 (2012).
[67] M. A. Bastarrachea-Magnani and J. G. Hirsch, *Phys. Scr.* **T160** 014005 (2014); *Phys. Scr.* **T160** 014018 (2014).

[68] A. Relaño, M.A. Bastarrachea-Magnani, S. Lerma-Hernández, arXiv:1608.03354 (2016); M. A. Bastarrachea-Magnani, A. Relaño, S. Lerma-Hernández, B. López-del-Carpio, J. Chávez-Carlos, and J. G. Hirsch, arXiv:1611.07863 (2016).